SENSITIVITY OF RADIO REFRACTIVITY TO MOISTURE AND TEMPERATURE AND ITS INFLUENCE ON RADAR RAY PATH

Jidong Gao[1], Keith Brewster[1] and Ming Xue[1,2]

[1]Center for Analysis and Prediction of Storms and

[2]School of Meteorology

University of Oklahoma

submitted to *Adv. Atmos. Sci*. August 2007

Corresponding author address:
Dr. Jidong Gao,
Center for Analysis and Prediction of Storms,
National Weather Center, Suite 2500,
120 David L. Boren Blvd, Norman, OK 73072
E-mail: jdgao@ou.edu

ABSTRACT

In this study, the sensitivity of radio refractivity to temperature and moisture is analyzed and the effects of vertical gradients in temperature and moisture on the propagation paths of electromagnetic waves of weather radar are examined for several sites across the United States using several years of sounding data from the National Weather Service. The ray path is important for identifying storm characteristics and for properly using the radar data in initializing numerical weather prediction models. It is found that during the warm season the radio refractivity gradient is more sensitive to moisture gradients than to those of temperature. Ray paths from the commonly accepted vertical ray path model are compared to a ray path computed from a stepwise ray tracing algorithm using data from actual soundings. For the sample of about 16,000 soundings examined, we find that only a small fraction of the ray paths diverge significantly from those calculated using a ray path model based on the standard atmosphere sounding. While the problem of ray ducting in the presence of a temperature inversion is fairly well known, we identify the presence of a strong vertical moisture gradient as the culprit in the majority of the cases where significant deviations occurred, a result consistent with our sensitivity analysis.

1. Introduction

The United States operational WSR-88D Doppler radar network (NEXRAD) is a vital tool for the real time detection and warning of hazardous weather (Crum and Albert 1993; Crum et al. 1998; Serafin and Wilson 2000). It is also an essential observing system for initializing non-hydrostatic, storm-resolving (i.e., horizontal grid spacing of order 1 km) numerical weather prediction (NWP) models (e.g., Lilly, 1990; Droegemeier 1990, 1997). Attempts to demonstrate such capability began early in the past decade (e.g., Sun et al. 1991), and subsequent efforts have been notably successful (e.g., Gao et al. 1998; Sun and Crook 2001; Weygandt et al. 2002a,b; Crook and Sun 2002; Xue et al. 2003; Brewster et al. 2003; Gao et al. 2004; Hu et al. 2006a,b).

To utilize the radar reflectivity and radial velocity data in real-time warning and quantitative precipitation estimation and to assimilate the data into NWP models, it is necessary to accurately determine the spatial locations of individual radar measurements. Because the propagation path of the electromagnetic waves can be affected by the refractivity of the atmosphere, the propagation path or the ray path is usually not a straight line. A suitable ray path equation is needed and the local direction of the path also affects the radial velocity forward operator that projects the velocity components on the model grid to the local radial direction in data assimilation systems.

Most early radar data assimilation studies used relatively simple ray path equations in the forward operator formulation, with the simplest one being based on the Cartesian flat-earth geometry (e.g., Gao et al. 1998, 2004; Weygandt et al. 2002a, b; Shapiro et al. 2003). The next level of sophistication is to use the four-thirds earth radius model (see, e. g., Doviak and Zrnic 1993, Gao et al. 2006) for the radar ray path calculations (e.g., Brewster 2003). This model takes into account the curvature of the earth but assumes that the atmosphere has a constant vertical

gradient of refractivity in the lower troposphere as determined from the U.S. Standard Atmosphere. In reality, the gradient of the refractivity is seldom constant and significant departures from the assumption exist when there are strong temperature inversions and/or large vertical moisture gradients. A better understanding of the sensitivity of the ray path to the gradient of refractivity and of the frequency that significant departures occur from the prediction of simple models is valuable to radar data quality control and radar data assimilation. In this study, the sensitivity of radio refractivity to temperature and moisture is first analyzed, the influence of atmospheric radio refractivity on the ray paths at locations representing four different climate regions of the United States is then examined using several years of sounding data from the National Weather Service.

The rest of this paper is organized as follows: In section 2, the four-thirds earth radius model for radar ray path calculations is briefly reviewed. An analysis of the sensitivity of refractivity to temperature and moisture variables is given in section 3. In section 4, a stepwise ray trace method is introduced. In section 5, the influence of atmospheric refractivity on the ray path at different geographical locations in the United States is examined using historic sounding data from National Weather Service. Finally, a summary and conclusions are given in section 6.

2. Ray path equations based on the four-thirds earth radius model

Under the assumption that temperature and humidity are horizontally homogeneous so that refractivity is a function of height above ground only, a formula can be derived (Doviak and Zrnic 1993) that expresses the ray path in terms of a curve following a sphere of effective radius

$$a_e = \frac{a}{1 + a\left(dn/dh\right)} = k_e a\,, \tag{1}$$

where a is the earth's radius and k_e is a multiplier which is dependent on the vertical gradient of refractive index of air, dn/dh. Here h is height above ground. When the U.S. Standard Atmosphere is considered, it is found that k_e is approximately equal to 4/3. This is often referred to as the "four-thirds earth radius model". The refractive index of air, n, is a function of air temperature, pressure and humidity and is usually taken, subject to certain assumptions, as (Beam and Dutton 1968),

$$N = (n-1)\times 10^6 = 77.6\frac{P}{T} + 3.73\times 10^5 \frac{e}{T^2}, \tag{2}$$

where P is air pressure (including water vapor pressure, in hPa), e is water vapor pressure (hPa), and T is air temperature (K). It is convenient to use the quantity N, defined as the atmosphere radio refractivity, instead of n. N represents the departure of n from unity in parts per million. N typically has a value of about 300 near the ground surface and its variations with the height, dN/dh, can be considered more conveniently.

The following two equations relate the height above ground, h, and the surface range (distance along the earth's surface from radar), s, to radar-measurable parameters, the slant path, r and radar elevation angle, θ_e (Doviak and Zrnic 1993),

$$s = a_e \sin^{-1}\left(\frac{r\cos\theta_e}{a_e + h}\right), \tag{3}$$

$$h = \left[r^2 + a_e^2 + 2ra_e \sin\theta_e\right]^{1/2} - a_e . \tag{4}$$

In Doviak and Zrnic (1993), it is also shown that if $r \ll k_e a$, and the coordinates x, y and z are related to the radar coordinates (r, θ_e, ϕ) by,

$$x \approx r\cos\theta_e' \sin\phi , \tag{5a}$$

$$y \approx r\cos\theta_e^{'}\cos\phi\,, \tag{5b}$$

$$z = h = (a_e^2 + r^2 + 2rk_e a\sin\theta_e^{'})^{1/2} - k_e a\,, \tag{5c}$$

where $\theta_e^{'}$, the angle between the radar beam and the earth's tangent plane below the data point, is the sum of two terms expressed as the following,

$$\theta_e^{'} = \theta_e + \tan^{-1}[r\cos\theta_e/(a_e + r\sin\theta_e)]\,. \tag{6}$$

From (5a) and (5b), one can easily derive the distance along the earth's surface as,

$$s^{'} \approx r\cos\theta_e^{'}\ . \tag{7}$$

Equation (7) is an approximation of the ray path equation (3). Equation (5c) uses exactly the four-thirds earth radius beam height equation (4).

3. Sensitivity analysis of refractivity to temperature and dewpoint

In Eq. (2), the first term on the right hand side is known as the dry term, the second term the moist term. The value of radio refractivity *N* can be computed from measurements of pressure, *P,* temperature, *T,* and water vapor pressure, *e*. Because in the troposphere the fractional decrease in *P* is larger than that in *T*, the variation of radio refractivity *N* with height, *dN/dh*, is usually negative. For the U.S. Standard Atmosphere, *dN/dh* is about –39.2 km^{-1}. If *N* decreases more (less) rapidly with height than the Standard Atmosphere, the beam may be refracted more (less), and in such cases, the height of a target may be overestimated (underestimated) by the four-thirds earth radius model. In an extreme condition, e.g., in the presence of a sharp refractivity gradient of about –150 km^{-1} below 100 m AGL (above ground level), a ray sent at a small positive elevation angle may actually decrease in height with range and eventually strike the earth surface.

Because the air pressure usually makes a rather stable contribution to the variation of N, we will only analyze the sensitivity of N to temperature and moisture. The amount of moisture in the air can be expressed in many forms. Four commonly used moisture variables are dewpoint temperature, T_d, water vapor pressure, e, relative humidity, and specific humidity. To ease comparisons with the sensitivity to temperature, we choose the dewpoint as the moisture variable for our sensitivity study. A commonly used approximate relation between dewpoint and water vapor pressure is Teten's formula (Krishnamurti 1986):

$$e = 6.11 \exp \frac{\alpha (T_d - 273.16)}{T_d - \beta}, \tag{8}$$

where for water α=17.26, β=35.86 and for ice α=21.87, β=7.66. Taking the leading-order variation of (8) with respect to dewpoint gives

$$\delta e = e \left(\frac{\alpha (273.16 - \beta)}{(T_d - \beta)^2} \right) \delta T_d, \tag{9}$$

where δe is the variation of water vapor, e, and δT_d is the variation of dewpoint.

By taking the leading-order of variation of the refractivity equation (Eq. 2) with respect to temperature and water vapor pressure, we have

$$\delta N = -\left(\frac{77.6P}{T^2} + \frac{2 \times 3.73 \times 10^5 e}{T^3} \right) \delta T + \frac{3.73 \times 10^5}{T^2} \delta e, \tag{10}$$

where δN is the variation of refractivity, and δT is the variation of temperature. Substituting (9) into (10), and letting

$$A \equiv \frac{\partial N}{\partial T} = -\left(\frac{77.6P}{T^2} + \frac{2 \times 3.73 \times 10^5 e}{T^3} \right), \tag{11}$$

$$B \equiv \frac{\partial N}{\partial T_d} = \frac{3.73 \times 10^5 (273.16 - \beta) \alpha e}{T^2 (T_d - \beta)^2}, \tag{12}$$

we have

$$\delta N = A\,\delta T + B\,\delta T_d \,. \tag{13}$$

It is obvious from (11) and (12), A<0 and B>0. These two terms reflect the sensitivity of refractivity to temperature and dewpoint respectively. Figures 1a and 1b show the variations of A and B as a function of base variables temperature and dewpoint, respectively, within a temperature range of -10 to 40 ^{0}C, a dewpoint range of -32.0 to 40 ^{0}C (or from about 10% to 100%- in terms of relative humidity) at a constant pressure of 1000 hPa. Figure 1c shows the absolute ratio between the variations with dewpoint (term B) and that of temperature (term A). It is clear from Fig. 1c that refractivity is more sensitive to dewpoint than regular temperature when the base temperature is high. Note especially that when the base temperature is at or above 30°C and the base dewpoint is greater than -16.0, the sensitivity of refractivity to dewpoint is 5 to 6 times greater in magnitude than that to temperature. When the low-level temperature is between 10 to 30°C, the temperatures typically found from spring to early fall, the sensitivity of refractivity to dewpoint is 2 to 4 times greater than to temperature. When the temperature is around 0°C, the winter situation, the sensitivities of refractivity to temperature and moisture variables are of the same magnitudes (see the low-left corner of Fig. 1a and b). Since A and B have opposite signs, the gradient of refractivity is usually almost constant during winter and at the upper levels of the atmosphere when and where air temperature is low. When the base pressure is set to 700 hPa, the pattern of sensitivity is very similar to that shown in Fig. 1, though values of term A and B are slightly smaller (not shown). Therefore, the above discussion is applicable for the entire depth of a typical planetary boundary layer, where the humidity has significant influence on the atmosphere.

Dividing (13) by δh, we get

$$\frac{\delta N}{\delta h} = A\frac{\delta T}{\delta h} + B\frac{\delta T_d}{\delta h}. \qquad (14)$$

Normally, both temperature and dewpoint decrease with the height, i.e., $\frac{\delta T}{\delta h} < 0$ and $\frac{\delta T_d}{\delta h} < 0$. So the temperature term makes a positive contribution to the rate of decrease in N but the moisture term makes a negative contribution. To satisfy the condition that the decrease in N with height exceeds a certain value (i.e., $\frac{\delta N}{\delta h}$ < -157 km^{-1}), and so that electromagnetic beams are bent toward the surface of the earth, i.e., for them to be trapped, either $\frac{\delta T}{\delta h}$ should be greater than zero, which happens in the inversion layers, or $\frac{\delta T_d}{\delta h}$ should be much less than zero, which happens when a very dry layer overlays a relatively moist layer.

To further quantify our analysis, given a basic state with relative humidity RH = 60%, temperature T = 17 ^{o}C and pressure P = 1000 hPa, we can calculate the values of the other base variables T_d = 11.7 ^{o}C, e = 13.7 hPa and N = 328.25. Substituting these values into (11) and (12), we get $A \equiv \frac{\partial N}{\partial T} = -1.34$ and $B \equiv \frac{\partial N}{\partial T_d} = 4.02$. These values indicate that a 1^{o}C change in temperature causes a 1.34 unit change in refractivity N; while a 1^{o}C change in dewpoint causes a 4.02 unit change in refractivity. Since variability on the order of few degrees is typical of both temperature and dewpoint in the lower atmosphere, we can therefore say that the radio refractivity is about three times more sensitive to dewpoint than to temperature near the surface for the above typical condition. This point will be further demonstrated in section 5. Among a large number of soundings that we examine in section 5, many of the most extreme deviations of ray paths from the four-thirds earth model are caused by large moisture gradients, usually when a

very dry layer is present above a moist boundary layer. From our discussion, it can also be concluded that it is easier to retrieve moisture variable than temperature from refractivity if it is observed by radars or satellites during the warm season. Weckwerth et al. (2005) showed an interesting result that under most daytime summertime conditions, refractivity from the radar measurements was representative of an about 250 m deep layer and could be useful for detecting low-level moisture boundaries.

4. A stepwise ray tracing method

In the last two sections, we presented a review on the ray path equations based on the four-thirds earth radius model, and analyzed the sensitivity of radio refractivity to temperature and dewpoint. In this section, the influence of different environmental thermodynamic profiles on the radar ray path is examined by using actual observed sounding data. To accurately estimate the radar ray path based on arbitrary sounding data, a stepwise ray tracing method is employed whose steps of calculation are as follows:

(a) Starting from the second gate from radar, for each radar measurement, calculate the refractivity N_{i-1} for the previous gate according to Eq. (2) based on the given thermodynamic profile where i is the index of the gates. Calculate the gradient of refractive index according to the differential of Eq. (2) with respect to beam height h,

$$\left.\frac{dn}{dh}\right|_{i-1} = 10^{-6} \left.\frac{dN}{dh}\right|_{i-1}. \qquad (15)$$

(b) Calculate $a_{e,i-1} = k_{e,i-1} a$ according to Eq. (1) using the gradient of refractive index from step (a) at the previous gate, i-1;

(c) Calculate the angle between the radar beam and the tangent plane below the data point, $\theta'_{e,i-1}$ using Eq. (6) for each radar gate;

(d) Finally, calculate the radar beam height h and the surface range s for gate i using formulas

$$\begin{aligned} h_i &= h_{i-1} + \Delta r \sin(\theta'_{e,i-1}), \\ s_i &= s_{i-1} + \Delta r \cos(\theta'_{e,i-1}), \end{aligned} \tag{16}$$

where Δr is gate spacing which is 250 m for U.S. operational WSR-88D radial velocity. Variables h_i and s_i are the beam height and surface distance for each gate, respectively. Steps (a) through (d) are repeated for successive gates until the last gate of each beam. Note that within this study that uses observed soundings, we assume that the sounding profile is representative of the vertical structure of the atmosphere within the entire radar range, which is not always true. For the data assimilation purpose, three dimensional gridded fields of temperature, moisture and pressure can be used to determine the local values of refractivity and further used in ray tracing calculations. The gridded fields can be from the analysis background or from a preliminary analysis that has already incorporated sounding and other non-radar observations.

5. Ray paths as determined from observed soundings

In this section, we examine the influence of radio refractivity on the ray path and its climatology in representative geographical regions of the United States, by calculating the ray paths for historic sounding data during a six-year period from January 1, 1998 to December 31, 2003 at four locations; namely, Oakland, California (OAK), Key West, Florida (EYW), Dulles Airport, Virginia (IAD) and Topeka, Kansas (TOP). These sites were chosen to represent the West Coast, Tropical Southeast, East Coast and Great Plains regions of the United States, respectively. Quality-controlled soundings were obtained from the online database of the NOAA Global Systems Division of the Earth System Research Laboratory.

For each sounding, the radar beam heights at all range gates, for the lowest 0.5º elevation, are calculated, using the four-thirds earth model and the stepwise ray-tracing method with the actual observed atmospheric profiles. The difference of the beam heights using these two methods is then divided by the corresponding beam width at the corresponding range, assuming a 0.93 degree beam width for the WSR-88D radars. The result can be regarded as relative beam height error. Table 1 shows the distribution of errors among six error intervals for the locations 50 km from a hypothetical radar site at the location and elevation of the radiosonde launch site. Among more than 4000 soundings for each site over the 6 year period, we find that the ray paths determined from the four-thirds earth radius model are in good agreement with the stepwise ray tracing method most of the time. More than 90% of the soundings result in relative beam height errors of less than 0.2. The ray paths determined from the four-thirds earth radius model are on average more accurate with the soundings from Oakland, California (OAK) than those from soundings of other sites; no relative errors greater than 0.8 are observed with the Oakland sounding profiles. The ray paths are less accurate with the soundings from Topeka, Kansas, with 0.4 % of soundings having relative beam height errors are greater than 1.

Table 2 shows the distribution of errors for the locations 120 km away from the virtual radar sites. For this distance, over 70% of soundings result in relative beam height errors of less than 0.2 for OAK and EYW. The number of soundings having beam height errors less than 0.2 is 91.3 % and 86.9 % for IAD and TOP, respectively, which are better than those for OAK and EYW sites. However, the numbers of soundings which result in relative beam height errors of above 1 are larger, at 0.8% and 2.4%, at IAD and TOP, respectively. As we might expect, range gates further away from the radar sites are more likely to have larger beam height errors using the four-thirds earth radius model due to the accumulation of error over distance and a greater

chance of encountering a layer with an extreme refractivity gradient. Thus radar data far away from radar sites are more prone to have location errors than data closer to radar sites.

From Table 2, we also notice that more than 20% of soundings result in beam height errors of between 0.2 and 0.8 for OAK and EYW, but less than 10% for IAD and TOP lie in the same range. No soundings from the OAK site and only 0.05% of soundings from EYW had relative errors greater than 1. However, 0.83% for IAD and 2.37% for TOP result in errors of 1 or greater. This indicates that while more soundings from IAD and TOP result in accurate ray path calculations based on the simple model, they also give rise to more cases which have very large relative errors, indicating more variability in the vertical refractivity at these sites.

Figure 2 shows the sounding, refractivity profile and the calculated ray path, for one of the worst cases from the TOP site. It is clear that the very strong moisture gradient found in this sounding is responsible for the large vertical refractivity gradient (Fig. 2a, b). The radar beam refracted downward toward the earth surface due to the layer of sharp refractivity gradient below the 1-km level. In this case, the gradient of radio refractivity is largely caused by the vertical variations in humidity. For this site, we also examined many other cases having large ray path deviations and in most of those cases, a large moisture gradient was found at the low levels that caused the beams to be refracted to the ground at a close radar range (as seen in Fig. 2c). Therefore, within the period examined, the beam ducting phenomena occurred more often in the Great Plains and East Coast areas of the U.S. than in the West Coast or Tropical Southeast because large moisture gradients near the surface occurred more frequently. In the Great Plains, this situation can be caused by high boundary-layer moisture from local sources or due to advection from the Gulf of Mexico that is overlaid with dry air having origins from the Rockies to the west. Similarly for Virginia, dry air advected from the Appalachians, or with a history of

subsidence, can often be found above a shallow layer of moist air near the ground with origins from the Atlantic Ocean.

As an illustration of a case that had a clear effect on the radar observations, Figure 3 shows a recent case study for Amarillo, Texas. A large moisture gradient and a temperature inversion near 1.2 km above sea level (roughly 1000 m AGL) are quite pronounced. The calculated beam is trapped in a layer just 1000 m above the ground (Fig. 3c). To show the effect on the radar data in this case, figure 4 shows the radar image at 13:47 UTC, 08 June 2005 from WSR-88D radar at Amarillo, Texas (KAMA). The beam might be partially or completely hitting ground targets in places where colors of orange, red or white are found in the figure, as indicated within the area denoted by the circle. Many pixels within the areas showing high reflectivity have been removed by the automated clutter filter (black adjacent to red or white areas).

Suppose that we require that the error in the beam height relative to the beam width be no more than 0.5 for the location estimate to be accurate enough for data assimilation purpose, then we can see from Tables 1 and 2 that the number of soundings which qualify for the use of the four-thirds earth radius model for the ray path calculation is well above 90%. However, beam ducting and strong departures from the four-thirds earth model do occur at small percentages, especially in the Great Plains and Eastern United States. Some of these could be found in situations preceding severe weather events – situations for which the WSR-88D radar data are most needed. Most of these phenomena are caused by large moisture gradients in the lower atmosphere. For this reason, quality control and data assimilation systems should check for such situations, and, when present, use the more accurate ray-trace method for beam height calculation and/or discard low-level data that may be contaminated by ground targets due to beam ducting and/or inaccurate height determination.

6. Summary and conclusions

Radar ray path equations are used to determine the physical location of each radar measurement for data display, radar-data based automated detection algorithms, quality control and data assimilation. To best use radar data, the accuracy of ray path calculations and the assumptions involved need to be examined thoroughly to see if significant deviations from typically used Standard-Atmosphere-based four-thirds effective earth radius model occur frequently. Such large deviations occur when a strong temperature inversion and/or large vertical moisture gradient exist. In this study, we first analyzed the sensitivity of radio refractivity to atmospheric temperature and moisture. It is shown that radio refractivity gradient is more sensitive to the moisture than to temperature; therefore moisture has a more significant influence on the radar ray path calculation than temperature.

To accurately calculate the radar ray path based on general sounding profiles, a stepwise ray tracing program is developed. The influence of atmospheric refractivity on the ray path is examined using a large number of historic soundings from four sites representing different geographical regions of the United States. For the soundings examined, 90 % of them result in small relative beam height errors when calculated using the standard-atmosphere-based four-thirds earth radius model and only a small fraction of ray paths thus calculated diverge significantly from those calculated based on true soundings using the ray tracing method. But these small fractions of deviations could occur more often in situations preceding severe weather. For many of the problematic cases examined, the vertical moisture gradient is found to be a more significant contributor. The results of this paper may provide a useful guidance to radar data quality control, as well as the assimilation of radar data into numerical weather prediction models.

Acknowledgments

This work was supported by US NSF grants ATM-0331756, ATM-0331594, ATM-0530814 and EEC-0313747, and by DOT-FAA grant NA17RJ1227-01. The first and third authors were also supported partially by Chinese NSF 40620120437.

References

Bean B. R. and E. J. Dutton, 1968: *Radio Meteorology*, Dover Publication, 435 pp.

Brewster, K.A., 2003: Phase-correcting data assimilation and application to storm scale numerical weather prediction. Part II: Application to a severe storm outbreak. *Mon. Wea. Rev.* **131***,* 493-507.

Crook, N. A., J. Sun, 2002: Assimilating Radar, Surface, and Profiler Data for the Sydney 2000 Forecast Demonstration Project**.** *J. Atmos. Oceanic Technol.*, **19**, 888–898.

Crum, T. D. and R. L. Albert, 1993: The WSR-88D and the WSR-88D operational support facility. *Bull. Amer. Meteor. Soc.*, **74,** 1669-1687.

Crum, T. D., R. E. Saffle, and J. W. Wilson, 1998: An Update on the NEXRAD Program and Future WSR-88D Support to Operations. *Wea. Forecasting*, **13**, 253–262.

Doviak, R.J. and D.S. Zrnić, 1993: *Doppler Radar and Weather Observations*, Academic Press, 2nd Ed., 562 pp.

Droegemeier, K. K., 1990: Toward a science of storm-scale prediction. *Preprint, 16th conf. on Severe Local Storms*, Kananaskis Park, Alberta, Canada, Amer. Meteor. Soc., 256-262.

——, 1997: The numerical prediction of thunderstorms: Challenges, potential benefits, and results from real time operational tests. *WMO Bulletin*, **46,** 324-336.

Gao, J**.**, M. Xue, Z. Wang and K. K. Droegemeier, 1998: The initial condition and explicit prediction of convection using ARPS forward assimilation and adjoint methods with WSR-88D data. Preprints, *12th Conf. Num. Wea. Pred.*, Phoenix, AZ, Amer. Meteor. Soc., 176-178.

Gao, J., M. Xue, K. Brewster, and K. K. Droegemeier 2004: A three-dimensional variational data assimilation method with recursive filter for single-Doppler radar, *J. Atmos. Oceanic. Technol.*, **21,** 457-469.

Gao, J., K. Brewster, M. Xue, 2006: A comparison of the radar ray path equation and approximations for use in radar data assimilation, *adv. Adv. Atmos. Sci.*, **23,** 190-198.

Hu, M., M. Xue, and K. Brewster, 2006: 3DVAR and cloud analysis with WSR-88D level-II data for the prediction of Fort Worth tornadic thunderstorms. Part I: Cloud analysis and its impact. *Mon. Wea. Rev.*, **134,** 675-698.

Hu, M., M. Xue, J. Gao, and K. Brewster, 2006: 3DVAR and cloud analysis with WSR-88D level-II data for the prediction of Fort Worth tornadic thunderstorms. Part II: Impact of radial velocity analysis via 3DVAR. *Mon. Wea. Rev.*, **134,** 699-721.

Krishnamurti, T. N., 1986: Workbook on numerical weather prediction for the tropics for the training of class I and class II meteorological personnel, published by World Meteorological Organization, No. 669, Geneva, Switzerland.

Lilly, D. K., 1990: Numerical prediction of thunderstorms - Has its time come? *Quart. J. Roy. Meteor. Soc.*, **116,** 779-798.

Serafin, R. J., and J. W. Wilson, 2000: Operational weather radar in the United States: Progress and opportunity. *Bull. Amer. Meteor. Soc*. **81**, 501-518.

Shapiro, A., P. Robinson, J. Wurman, and J. Gao, 2003: Single-Doppler velocity retrieval with rapid-scan radar data, *J. Atmos. Oceanic. Technol*. **20**, 1758-1775.

Sun, J., D. W. Flicker, and D.K. Lilly, 1991: Recovery of three-dimensional wind and temperature fields from simulated single-Doppler radar data. *J. Atmos. Sci.,* **48**, 876-890.

Sun, J. and N. A. Crook, 2001: Real-time low-level wind and temperature analysis using single WSR-88D data. *Wea. Forecasting*., **16**, 117-132.

Weckwerth, T. M., C. R. Pettet, F. Fabry, S. Park, M. A., LeMone, and J. W. Wilson, 2005: Radar refractivity retrieval: Validation and application to short-term forecasting. *J. Appl. Meteorol*., **44**, 285-300.

Weygandt, S. S., A. Shapiro and K.K. Droegemeier, 2002a: Retrieval of initial forecast fields from single-Doppler observations of a supercell thunderstorm. Part I: Single-Doppler velocity retrieval. *Mon. Wea. Rev,* **130**, 433-453.

Weygandt, S.S., A. Shapiro and K.K. Droegemeier, 2002b: Retrieval of initial forecast fields from single-Doppler observations of a supercell thunderstorm. Part II: Thermodynamic retrieval and numerical prediction. *Mon. Wea. Rev.*, **130**, 454-476.

Xue, M., D.-H. Wang, J. Gao, K. Brewster, and K. K. Droegemeier, 2003: The Advanced Regional Prediction System (ARPS), storm-scale numerical weather prediction and data assimilation. *Meteor. Atmos. Physics*. **82**, 139-170.

List of figures

List of Tables

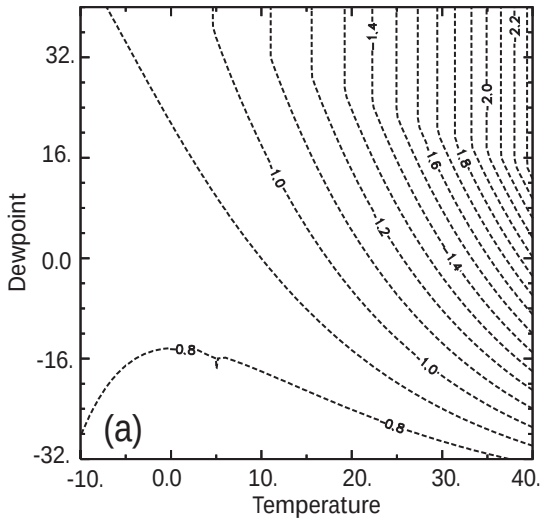
Dewpoint
32.
16.
0.0
-16.
-32.
-10.
0.0
10.
20.
30.
40.
Temperature
(a)
0.8
1.0
1.2
1.4
1.6
1.8
2.0
2.2

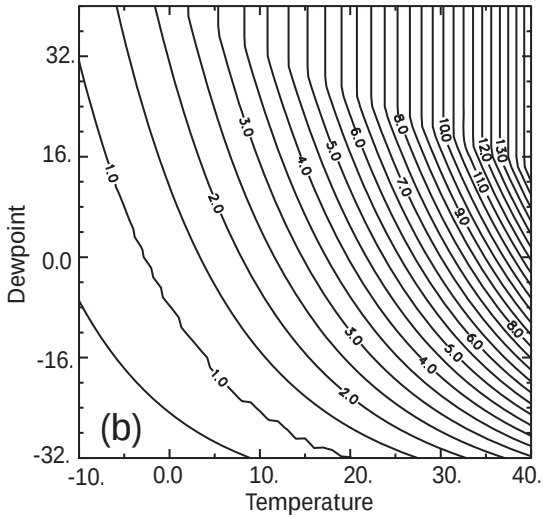
Dewpoint
32.
16.
0.0
-16.
-32.
-10.
0.0
10.
20.
30.
40.
Temperature
(b)
1.0
2.0
3.0
4.0
5.0
6.0
7.0
8.0
9.0
10.0
11.0
12.0
13.0

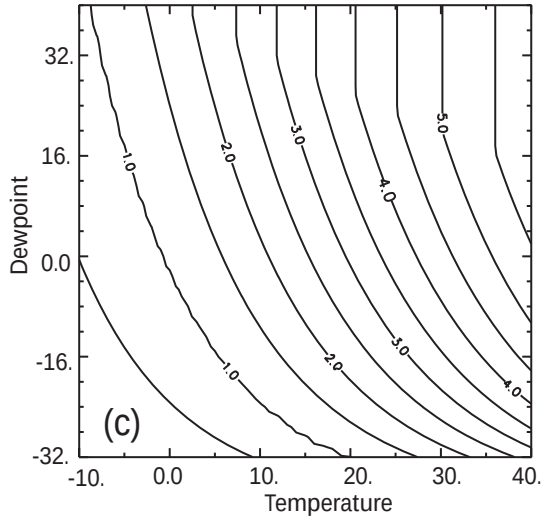
Dewpoint
32.
16.
0.0
-16.
-32.
-10.
0.0
10.
20.
30.
40.
Temperature
(c)
1.0
2.0
3.0
4.0
5.0

Figure 1. The sensitivity of refractivity to temperature indicated by the contours of $A \equiv \frac{\partial N}{\partial T}$ in (11) (a), and to dewpoint indicated by the contours of $B \equiv \frac{\partial N}{\partial T_d}$ in (12) (b), and the absolute ratio between B and A (c).

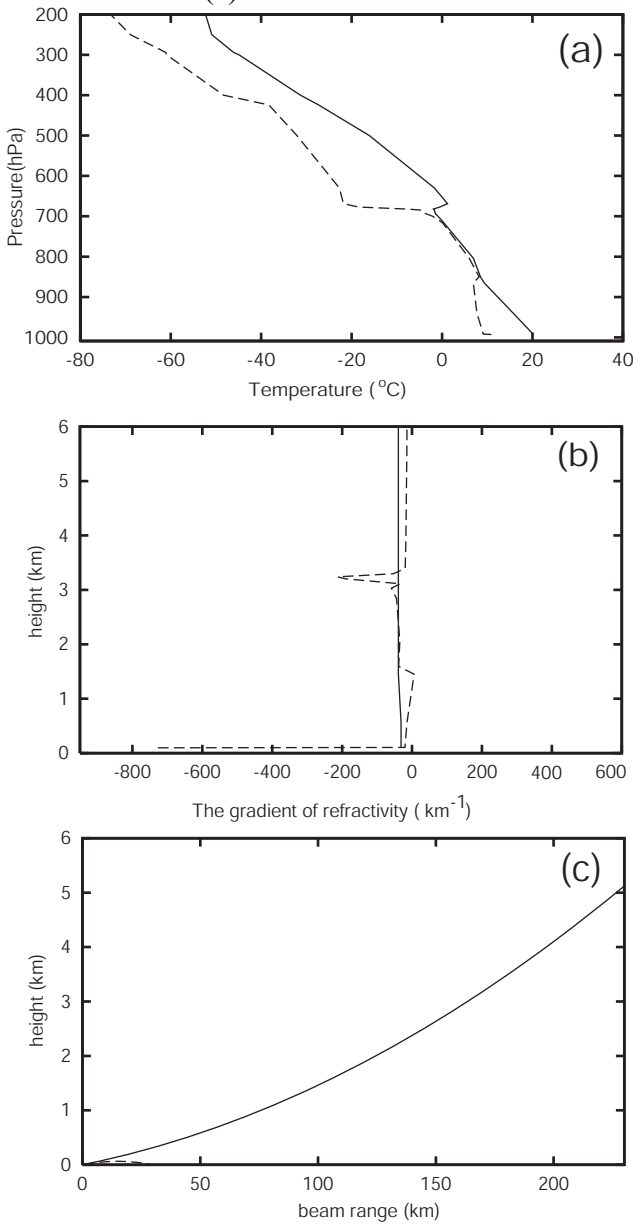

Figure 2. (a) The temperature (solid) and dewpoint (dashed) profiles, (b) the refractivity gradient profiles (km^{-1}) calculated from the Standard Atmosphere (solid) and from the observed sounding (dashed), and (c) the radar ray paths calculated for the 0.5º

elevation using the Standard Atmosphere (solid) and actual sounding and ray tracing method (dashed), for 0000 UTC, May 3, 1999 at Topeka, Kansas (TOP).

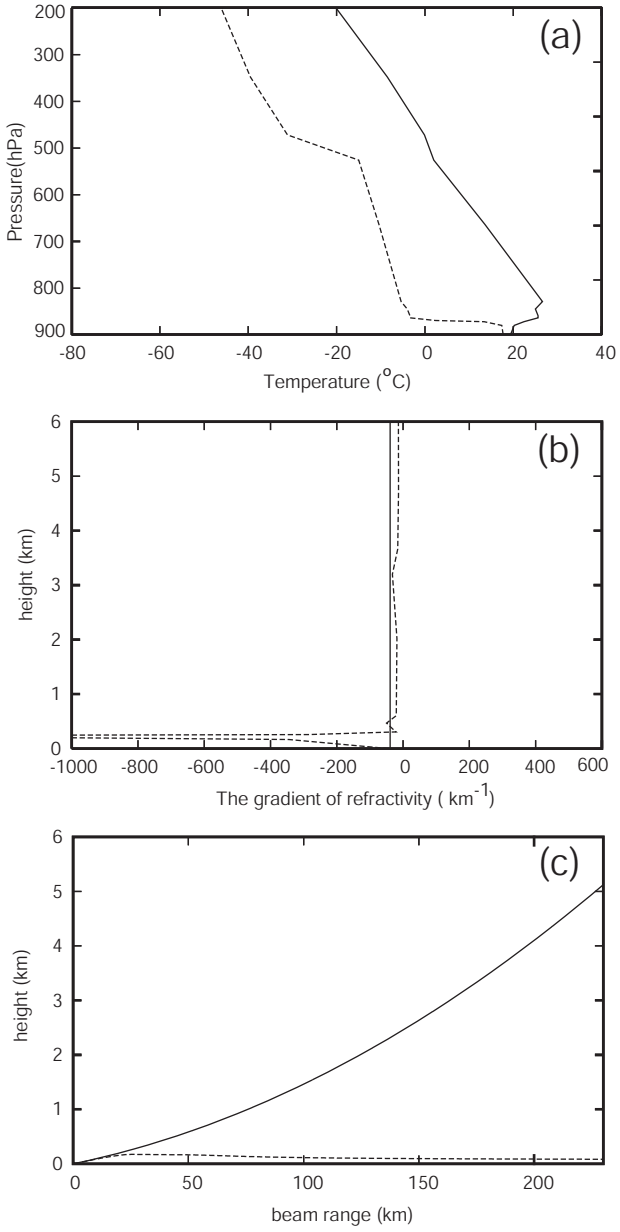

Figure 3. As Fig. 2, but for 1200 UTC, June 8, 2005 at Amarillo ,Texas.

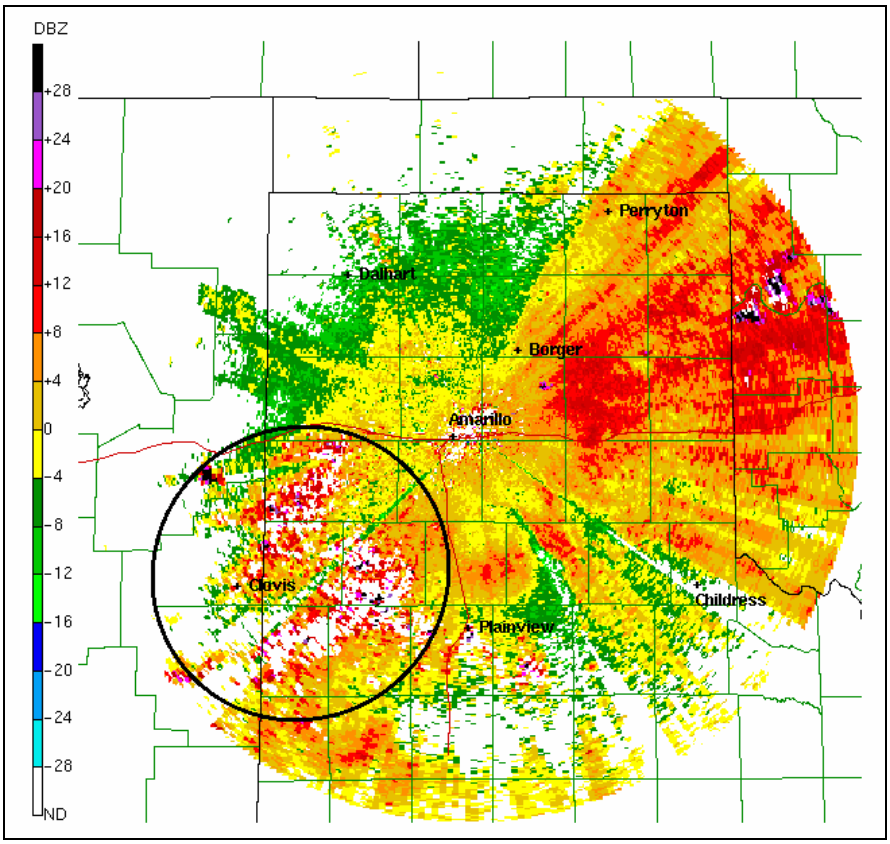

Figure 4. Radar reflectivity image at 13:47 UTC, June 08, 2005 for KAMA at Amarillo, Texas.

Table 1. Distribution of relative beam height errors among 6 error intervals for locations 50 km from the radar site.

Raob Sites	Obs. No.	Error Distributions (%)					
		[0 0.2]	[0.2 0.4]	[0.4 0.6]	[0.6 0.8]	[0.8 1.0]	[1.0 above]
OAK	4234	94.31	4.65	0.92	0.12	0.00	0.00
EYW	4202	94.10	5.02	0.79	0.05	0.00	0.05
IAD	4088	97.31	0.86	1.10	0.05	0.44	0.24
TOP	4253	93.63	3.74	1.27	0.75	0.19	0.42

Table 2. **Distribution of relative beam height errors among 6 error intervals for locations 120 km from the radar site.**

Raob Sites	Obs. No.	Error Distributions (%)					
		[0 0.2]	[0.2 0.4]	[0.4 0.6]	[0.6 0.8]	[0.8 1.0]	[1.0 above]
OAK	4234	76.17	4.82	7.58	10.01	1.42	0.00
EYW	4202	71.68	11.61	7.38	8.02	1.26	0.05
IAD	4088	91.34	3.69	1.71	1.32	1.10	0.83
TOP	4253	86.93	5.48	1.98	2.66	0.59	2.37